European Geothermal Congress 2013
Pisa, Italy, 3-7 June 2013

Organised by Co-produced with Supported by Main Sponsor

Applied Thermo-Hydro-Mechanical coupled modelling of geothermal prospection in the northern Upper Rhine Graben

Wolfram Rühaak, Ingo Sass.

Technische Universität Darmstadt, Institute of Applied Geosciences, Chair of Geothermal Science and Technology, Schnittspahnstrasse 9, D - 64287 Darmstadt, Germany

ruehaak@geo.tu-darmstadt.de

Keywords: THM coupled modelling, induced seismicity, EGS, Upper Rhine Graben.

ABSTRACT

Several geothermal power plants are planned for one of the most promising regions in Germany, the Upper Rhine Graben (URG). Induced seismicity can have a strong impact on the viability of such projects. For instance at the Basel/Switzerland Deep Heat Mining site, located at the southern end of the URG, after massive hydraulic fracturing in 2006/2007 several earthquakes with magnitudes of up to 3.4 occurred. An expert report on this seismicity has led to a final stop of the project. To prevent other geothermal projects from this fate a prognostic of possible induced seismicity and measures to limit the maximum magnitude are currently one of the most important geothermal research topics.

Based on a geometric GOCAD model of the German federal state Hessen, covering the northern part of the URG, a large scale heat transport model was developed. For regions where geothermal exploration is planned, coupled thermo-hydro-mechanical (THM) models can be computed. The THM modelling is based on a FEFLOW model for the thermo-hydro coupling together with a plug-in for the (linear elastic) mechanical coupling.

The approach is demonstrated exemplarily for a site, using literature data.

1 INTRODUCTION

A numerical code for solving linear elasticity, based on the Finite Element Method (FEM) in 3D has been developed (Rühaak et al., 2012a). At its current state it is intended to be coupled into existing 3D flow- and heat-transport codes to enable a hydro-mechanical and thermo-hydro-mechanical coupled modeling. A stand-alone version may be developed in future.

The general concept of THM coupled modelling is shown in Fig. 1. The current status in thermo-hydro-mechanical-chemical (THMC) coupled modelling was recently reviewed by Rutqvist (2011). Besides commercial all-in-one solutions (e.g. COMSOL Multiphysics, ABAQUS, ANSYS), a coupling of TOUGH2 with additional mechanical codes is often used (see Rutqvist, 2011). Furthermore OpenGeoSys (Kolditz et al., 2012) should be named for a research code with THMC capabilities. The code presented here is LGPL licensed open source and coupled to the commercial software FEFLOW (DHI-WASY, 2012). FEFLOW is one of the most used programs for groundwater, mass- and heat-transport modeling worldwide. It is endowed with a very user friendly and powerful user interface and besides of the parallelized (OpenMP) computational core it has also powerful pre- and post-processing capabilities, including 2D and 3D GIS data, to name some. FEFLOW is by default able to compute thermo-hydro-chemical (THC) coupled processes. By adding the newly developed mechanical plug-in it becomes a THMC simulator.

2 THERMO-HYDRO-MECHANICAL COUPLING

2.1 Hydro-mechanical coupling

The mechanical interaction between groundwater and the porous geologic media it permeates is central to the phenomenon of groundwater flow (Ingebritsen et al., 2006). Calculations which take this interaction into account are called hydro-mechanically (HM) coupled.

Different types of mechanical behavior are of relevance. In the subsurface, typically described as porous media, often only elastic dilatation is taken into account, not fracture.

Although no materials are actually linearly elastic over a wide range of stresses, elastic constitutive models are mostly sufficiently accurate for rock mechanics (Kolditz et al., 2012).

The theory describing the elastic behaviour of porous media is called poroelasticity. A general introduction into the theory of poroelasticity is given by Wang (2000). The theory consequently addresses the transient coupling between the deformation of rock and fluid flow within the rock. Different mathematical approaches are available; see Verruijt (1969), Smith & Griffiths (1988), Leake & Hsieh (1997), Hsieh (1997), Ingebritsen et al. (2006).

In the case of hydro-mechanical coupling it requires the solution of the groundwater flow (Darcy equation)

and the mechanical behavior described for instance following Biot (1941). For thermo-coupling additionally the heat- and mass-transport equations have to be coupled dynamically (Figure 1).

Two basic phenomena underlie poroelastic behavior (Wang, 2000):

- Solid-to-fluid coupling occurs when a change in applied stress produces a change in fluid pressure or fluid mass.
- Fluid-to-solid coupling occurs when a change in fluid pressure or fluid mass produces a change in the volume of the porous material.

2.2 Thermo Coupling

In the last years the inclusion of thermal effects into the theory of hydro-mechanical (HM) coupling has become more and more of relevance (e.g. Lee & Ghassemi, 2011). Important issues are for instance the modelling of the thermo-mechanical (TM) processes in nuclear waste disposals.

Thermo-hydro-mechanical induced stress-strain also has an impact on processes related to the usage of geothermal energy. For computing such processes numerically on the respective relevant scales, stress-strain relationships resulting from fluid pressure and temperature have to be computed and coupled to the regional flow and transport regime dynamically.

In case of thermo-hydro-mechanical (THM) coupling application examples are for instance the productivity of geothermal doublet systems with one pumping well and one injection well, which can be influenced due to mechanical changes and a related change of the hydraulic conductivity (Bundschuh & Suárez-Arriaga, 2010).

A general review with respect to THM coupled processes is given in Wang et al. (2009), Watanabe et al. (2010) and Kolditz et al. (2012).

Thermo-mechanical coupling is mainly working only in one direction as thermal expansion induces volume changes of the rock (similar to pore pressure changes in case of hydro-mechanical coupling); vice versa the mechanics do not alter the temperature directly but only due to changes of the (convective) flow field.

As mentioned before chemical coupling is possible but is not discussed here.

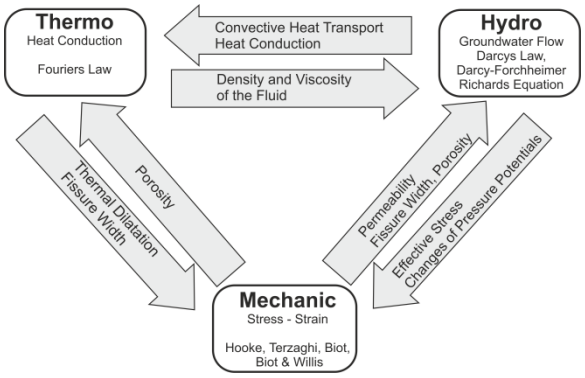

Figure 1: Thermo-hydro-mechanical coupling approach and the respective constitutive laws.

2.3 THM Continuity equations

The following continuity equations have to be solved (see Bear, 1972, Diersch & Perrochet, 1999, Alberty et al., 2002, Ingebritsen et al., 2006, Rühaak et al, 2008):

Groundwater flow

$$S_S \frac{\partial h}{\partial t} = \nabla \cdot (\mathbf{K} \nabla h) + \alpha_b \frac{\partial \varepsilon_{vol}}{\partial t} \qquad (1)$$

Darcy's law

$$\mathbf{q} = -\mathbf{K} \cdot \nabla h \qquad (2)$$

Coupled conductive and convective heat-transport

$$(\rho c)_g \frac{\partial T}{\partial t} = \nabla \cdot \left(\boldsymbol{\lambda} \nabla T - \rho_f c_f \mathbf{q} T \right) \qquad (3)$$

Linear elasticity equation

$$(\Lambda + \mathrm{M}) \mathit{grad\ div}\, \mathbf{u} + \mathrm{M} \nabla^2 \mathbf{u} = -\mathbf{f} \qquad (4)$$

Stress-strain relationship

$$\begin{bmatrix} \sigma_x \\ \sigma_y \\ \sigma_z \\ \tau_{xz} \\ \tau_{yx} \\ \tau_{zy} \end{bmatrix} = \begin{bmatrix} \Lambda+2\mathrm{M} & \Lambda & \Lambda & 0 & 0 & 0 \\ \Lambda & \Lambda+2\mathrm{M} & \Lambda & 0 & 0 & 0 \\ \Lambda & \Lambda & \Lambda+2\mathrm{M} & 0 & 0 & 0 \\ 0 & 0 & 0 & \mathrm{M} & 0 & 0 \\ 0 & 0 & 0 & 0 & \mathrm{M} & 0 \\ 0 & 0 & 0 & 0 & 0 & \mathrm{M} \end{bmatrix} \begin{bmatrix} \varepsilon_x \\ \varepsilon_y \\ \varepsilon_z \\ 2\gamma_{xz} \\ 2\gamma_{yx} \\ 2\gamma_{zy} \end{bmatrix} \qquad (5)$$

Where n is porosity (-), ρ is density (kg m^{-3}), g is gravity (m s^{-2}), h is hydraulic head (m), S is storage coefficient (m^{-1}), K is the hydraulic conductivity tensor (m s^{-1}), α_b (-) is an empirical constant (Biot, 1941), $\partial \varepsilon_{vol} / \partial t$ is the time rate of change of volumetric strain (s-1), **q** is the Darcy velocity (m s^{-1}), $(\rho c)_g$ is the bulk volumetric heat (J K^{-1} m^{-3}), T is temperature (°C), λ is the thermal conductivity tensor (W m^{-1} K^{-1}), index f denotes fluid properties, υ is Poisson's ratio (-), u is the displacement vector (m), σ are stresses (MPa), ε are strains (-),τ and γ denote shear stress and shear strain, respectively (MPa). Indexes x, y, z denote the respective Cartesian

directions. **f** is the loading force (N), typically resulting from the pore pressure.

Λ is Lamé's first parameter[1],

$$\Lambda = \frac{E\upsilon}{(1+\upsilon)(1-2\upsilon)} \quad (6)$$

M is the second (MPa), identical to the shear modulus, often denoted as G.

$$\mathrm{M} = \frac{E}{2(1+\upsilon)} \quad (7)$$

E is Young's modulus (MPa).

As a convention in the presented code pressure values, like pore pressure, loading forces and the Young's and the shear modulus have to be given in MPa.

In Eq. (1) the last term $\alpha_b \partial\varepsilon_{vol}/\partial t$ reflects the volume change of the porous medium, which is equivalent to adding or removing fluid. It can therefore be seen as a fluid source/sink term (Neuzil, 2011) and is handled this way in the presented coupling approach, substituting the strain by the volume change (dilation) of the respective elements during the previous time step (Ahola et al., 1996):

$$\alpha_b \frac{\partial\varepsilon_{vol}}{\partial t} \cong \alpha_b n \frac{V_o - V}{V_o}\frac{1}{\Delta t} \quad (8)$$

Here V_0 is the element volume at time zero while V is the element volume after displacement; n means porosity (-). This source/sink of fluid Q_t (s^{-1}) is added to the groundwater flow equation at time t as

$$Q_t \cong \alpha_b n \frac{V_{t-1} - V_t}{V_{t-1}}\frac{1}{\Delta t}, \quad (9)$$

where subscript t^{-1} refers to the result of the previous time step. Δt is the current time step size.

Within the FEFLOW IFM plug-in for this a call to the IFM API (application programming interface) changes the sink/source term of groundwater flow equation (Eq. 1).

The loading or volume forces (see Eq. 4)

$$\mathbf{f} = \alpha_b \rho_f g V \nabla h \quad (10)$$

are evaluated as a vector in the centre of gravity. They represent the pore-pressure (Ingebritsen et al., 2006):

$$\sigma_{\mathrm{eff}} = \sigma_{\mathrm{total}} - p_{\mathrm{pore}} \quad \sigma_{eff} = \sigma_{total} - p_{pore} \quad (11)$$

The head gradient ∇h is computed using a code from Abriola & Pinder (1982).

In case of a thermo-hydro-mechanical problem the expansion of the rock matrix due to temperature changes has to be taken into account. Changes of the fluid properties are not discussed here because they are handled by FEFLOW directly (for details see Diersch & Kolditz, 2002). The volume of a solid increases or decreases with temperature changes and homogenous bodies expand evenly in all directions by increasing temperatures. If a deformation is not possible the internal stresses increase or decrease with temperature changes (Kolditz et al., 2012). This unidirectional stress **f'** is added to the volume force following Ahola et al. (1996):

$$\mathbf{f}' = D\beta\Delta T \quad (12)$$

D is the bulk modulus according to:

$$D = \Lambda + \frac{2\mathrm{M}}{3} \quad (13)$$

Where β is the volumetric thermal expansion coefficient (K^{-1}).

Coupling occurs among the equations because pore pressure appears in the force equilibrium equations, and because volumetric strain appears in the fluid-flow equation (Wang, 2000).

Due to the mechanical deformation a non-linear system results which requires additional treatment to obtain convergence. The strain modifies the fluid-pressure, while the fluid-pressure is a force which is biasing the strain. Compared to the other TH coupled processes mechanical compaction can be seen as an instantaneous process (Kolditz et al., 2012). Convergence is obtained by performing additional inner iterations to minimize the variance of the steady-state strain. As stress and strain have a negligible impact on the temperature (Kolditz et al., 2012), a backward coupling is not performed.

Due to the strain a change of the porosity and permeability is likely. This can be taken into account by reducing the porosity linearly with the change of volume and a simultaneous change of the permeability in accordance to the porosity. For the latter the application of a fractal law (Pape et al., 1999) is a straightforward approach:

$$k = 31n + 7463n^2 + 191(10n^{10}) \quad (14)$$

k denotes here the intrinsic permeability (m^2) which is connected with the hydraulic conductivity *K* by

$$\mathrm{K} = \frac{\mathrm{k}\rho\mathrm{g}}{\mu} K = \frac{k\rho g}{\mu}, \quad (15)$$

here μ is the dynamic viscosity of the fluid

(kg m^{-1} s^{-1}). However, in case of the following examples no porosity and permeability changes have been applied.

2.4 3D Finite Element implementation for linear elasticity

Flow and heat transport are regularly computed with FEFLOW. In an additional IFM plug-in, corresponding stress and strain is computed.

[1] To avoid confusion with the hydraulic and thermal parameters large Greek letters are used for the Lamé parameters, instead of the more common small ones.

The routines for solving the Navier-Lamé equation for linear elasticity are part of the ffp library (*free finite element program*); while the plug-in itself is called mcf (*Mechanical Coupling FEFLOW*). All routines are open source (LGPL[2]) and available from http://sourceforge.net/projects/ffp/.

Boundary conditions (Neumann – scalar weight and Dirichlet – vectorial displacement) as also the elemental parameters (Lamé's first and second parameters) can conveniently be assigned using the graphical user interface of FEFLOW and so called 'user data'.

For the 3D solution a tetrahedron based FEM approach is used, other element types are currently not supported. The FEM implementation is based on Alberty et. al (2002). The code is written in standard ANSI/ISO C++.

The most common geometrical element type used in FEFLOW is a pentahedron (in other words a wedge or a triangular prism). Tetrahedrons are not supported. The plug-in generates three tetrahedrons for each FEFLOW pentahedron (for details see Dompierre et al., 1999). For this TetGen (Si & Gärtner, 2005) is used. The motivation for using TetGen for this simple task is to enable future subgrid approaches more easily.

For solving the direct Intel PARADISO solver is implemented. A conjugate gradient solver, using the GPU (using NVIDIA's CUDA functions) is currently under development.

FEFLOW does allow a moving mesh in vertical but not in horizontal direction. The mcf plug-in therefore does not modify the problems geometry according to the actual displacement. Besides of the limitations of FEFLOW this is mainly justified by the relative small amounts of displacement. The bias introduced by this approach should be neglect able in most cases. However, future developments will include a 3D moving mesh. For this the result data will be stored in the VTK format.

2.5 Benchmarks & Verifications

An important part in developing numerical programs is to verify the code in order to ensure agreement of the results with known solutions.

The increased effective stress due to pumping results in compaction of the aquifer. The reduction of pore space results in an increased flow rate and the solid frame compacts further. Accordingly the stress field changes and fluid flow gradients affect each other mutually.

For the benchmark a setup in accordance with Leake & Hsieh (1997) is used: Three sedimentary layers overlay impermeable bedrock in a basin where faulting creates a bedrock step near the mountain front. The sediment stack totals 440 m at the deepest point of the basin (x = 0 m) but thins to 120 m above the step (x > 4000 m). The total width is 5200 m. The top two layers of the sequence are each 20 m thick. The first and third layers are aquifers; the middle layer is relatively impermeable to flow. The materials are homogeneous and isotropic within a layer. The flow field is initially at steady state, but pumping from the lower aquifer reduces hydraulic head by 6 m per year at the basin centre.

As shown in Figure 2, the polygon represents an aquifer composed of different sediments. Edge E represents a drainage border, where the hydraulic head is lowering with a rate of 6 m per year. The total simulation time is 10 years. The used parameters and boundary conditions are given in Table 1 and Table 2.

Table 1: Parameters used for the Leake & Hsieh (1997) example.

Value	Aquifer	Confining	Unit
S_s	$1 \cdot 10^{-6}$	$1 \cdot 10^{-5}$	m^{-1}
K	$2.89 \cdot 10^{-4}$	$1.16 \cdot 10^{-7}$	$m\ s^{-1}$
$\Lambda = M$	320	32	MPa
υ	0.25		
α_b	1		

Table 2: Hydraulic and mechanical boundary conditions.

Boundary Conditions	Mechanical	Hydraulic
A	fixed	flux = 0 $m\ s^{-1}$ (Neumann)
B	free	flux = 0 $m\ s^{-1}$ (Neumann)
C	free	$h = h_0$
D	free	$h = h_0$
E	free	h = h(t)

The result shown in Figure 3 is in good accordance with the original result by Leake & Hsieh (1997). Differences are mainly due to a different mechanical boundary condition at boundary E. Originally here a so called roller boundary condition (only displacement in vertical direction is possible) is used. However, the code presented here does not support such type of boundary condition. Therefore the boundary can also move horizontally and – because the model is in fact 3D – also in the direction perpendicular to the view.

3 HESSEN 3D

Based on a 3D structural GOCAD model (Arndt et al. 2011) and an extended geothermal database (Bär et al. 2011) of the federal state Hessen/Germany (Figure 4) the subsurface temperature distribution was computed (Rühaak et al., 2012b). Since subsurface temperature data for great depth are typically sparse, two different approaches for estimating the spatial subsurface temperature distribution have been used.

[2] http://www.gnu.org/copyleft/lesser.html

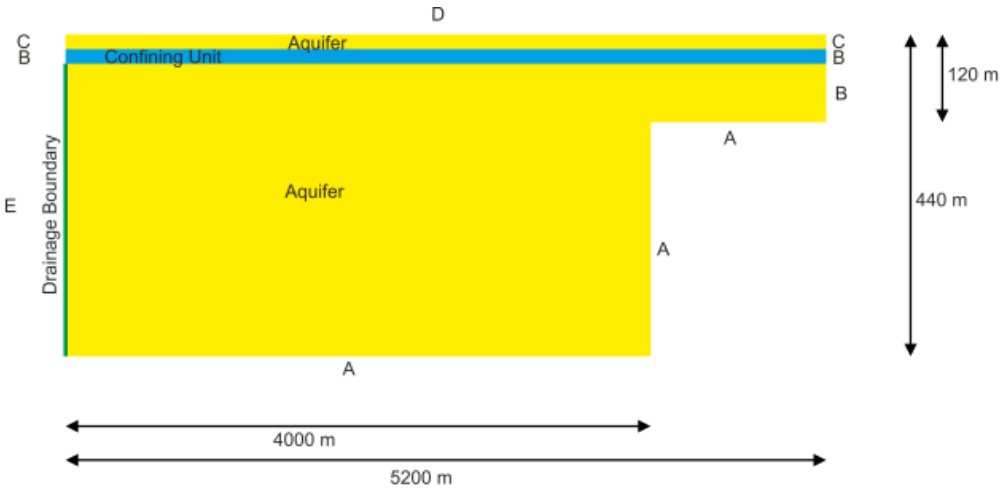

Figure 2: The setup of the benchmark example following Leake & Hsieh (1997). (View is vertically 5-times exaggerated.)

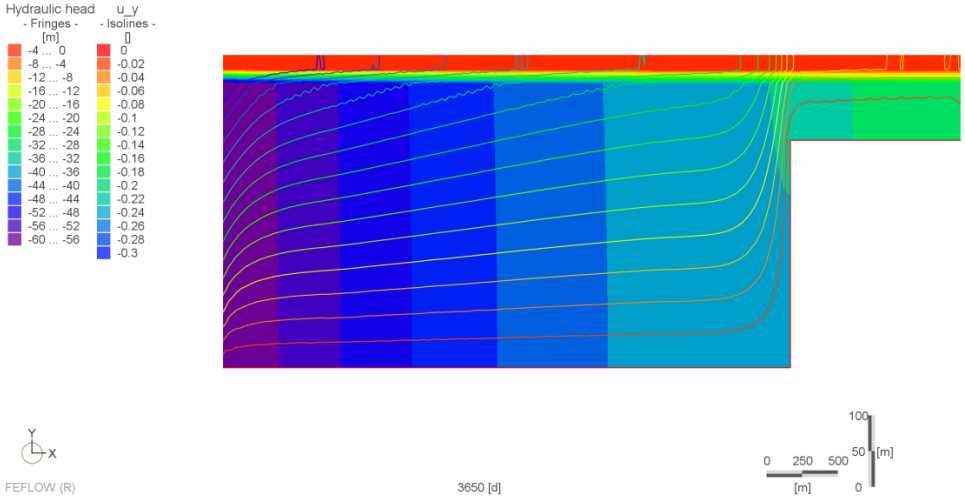

Figure 3: Result of the Benchmark. Filled contours show the head while the isolines depict the displacement (m) in vertical direction. (View is vertically 5-times exaggerated.)

Figure 4: The Hessen 3D GOCAD Model (Bär et al., 2011).

3.1 3D Numerical Modeling

One classical approach for estimating the subsurface temperature distribution is the numerical computation of a 3D purely conductive steady state temperature distribution (Rühaak et al. 2010). The numerical model is based on measured thermal conductivity data for all relevant geological units and surface temperatures (Sass et al. 2011). The basal heat flow is estimated following the approach of Arndt et al. (2011). It is spatially varying from 65 mW m^{-2} to 95 mW m^{-2} according to the presumed Moho depth using data from Dèzes & Ziegler (2001).

The model is calibrated using continuous temperature logs. Only conductive heat transfer is considered since not enough data for convective heat transport at great depths are available.

The assigned parameters are given in Table 3.

The result is shown in 3D Figure 5. In Figure 6 the results for 500 m and 1000 m below the surface are

shown, respectively. The fit of the modelled logs is very good in the areas that are influenced by convective heat transport; within such areas the fit is poor.

Table 3: Parameters used for the conductive heat transport model.

Nr	Model-Unit	n	λ (W m^{-1} K^{-1})	ρc (J m^{-3} K^{-1})
1	Tertiary (Vulcanite)	0.016	1.84	$2.0 \cdot 10^6$
2	Muschelkalk	0.043	2.10	$1.8 \cdot 10^6$
3	Buntsandstein	0.135	2.97	$1.8 \cdot 10^6$
4	Zechstein	0.115	2.55	$2.1 \cdot 10^6$
5	Rotliegend	0.089	2.42	$2.0 \cdot 10^6$
6	N'metamorphic Basement	0.036	2.81	$1.8 \cdot 10^6$
6	S' crystalline Basement	0.002	2.40	$2.1 \cdot 10^6$

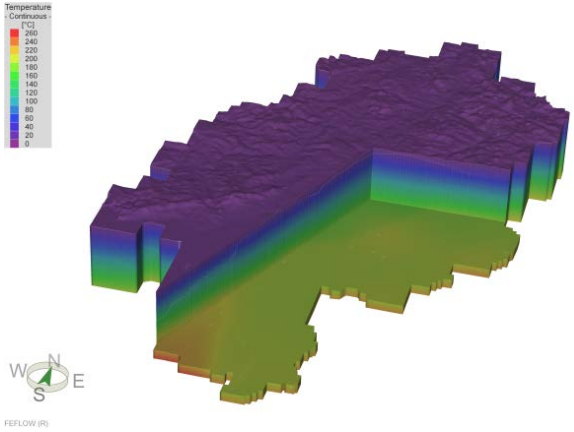

Figure 5: The FEFLOW heat-transport model.

3.2 3D Kriging of Temperature Measurements

The other approach to estimate the subsurface temperature distribution is by 3D ordinary Kriging. Here a modified approach is applied where the quality of the temperature measurements (see Table 4) is taken into account (Rühaak 2006, Rühaak 2012). A difficult but important part is to derive good variograms for the horizontal and vertical direction. The variograms give necessary information about the spatial dependence of the data. The Hessen 3D model was subdivided into submodels according to the different geostructural regions. The horizontal variogram (Figure 7) is based on all data from the Odenwald and Sprendlinger Horst, Hanau Seligenstädter Senke, Hessen North-East and Schiefergebirge. Data from the Mainzer Becken and the Upper Rhine Graben are not used for this variogram as they are strongly disturbed by convective heat transport. The vertical variogram (Figure 8) is based on data from all regions but only high quality measurements from continuous logs are used. In Figure 9 the results for 500 m and 1000 m below the surface are shown, respectively. Similarities where conduction is dominant and differences where convection is strong can be seen while comparing with Figure 6.

3.3 Summary of the Hessen 3D temperature modeling results

Differences in the predicted subsurface temperature distribution are mainly related to convective processes, which are reflected by the interpolation result, but not by the numerical model. Therefore, a comparison of the two results is a good way to obtain information about flow processes in such great depth. This way an improved understanding of the heat transport processes within this mid enthalpy geothermal reservoirs of Hessen (1,000 m – 6,000 m) is possible.

The computation of a fully coupled flow and heat transport model would be ideal. However, due to the small number of data any such result lacks reliability.

To obtain the theoretical variograms necessary for the Kriging is a difficult task. Especially the quality of the horizontal semi-variogram is poor. However, it is sufficient for obtaining a reasonable spatial temperature distribution. Especially the inclusion of a weighting algorithm (Rühaak, 2013, http://sourceforge.net/projects/jk3d/) helps to improve the Kriging result as artefacts due to low quality measurements only have a small impact - where high quality data are available.

The combination of both approaches might result in a temperature model with a good fit to the given temperature measurements as well as a good extrapolation of subsurface temperatures in depths where no data is available. Such a model increases the quality of geothermal potential predictions compared to purely numerical or geostatistical approaches.

In this study the paleoclimate signal was not taken into account, which is relevant especially for depths up to approximately 1000 m. Also heat production was neglected for the numerical model. Both aspects as well as the influence of fault zones as conduits for convective heat transport should be addressed in future work. Additionally the impact of a temperature dependent thermal conductivity should be studied in future.

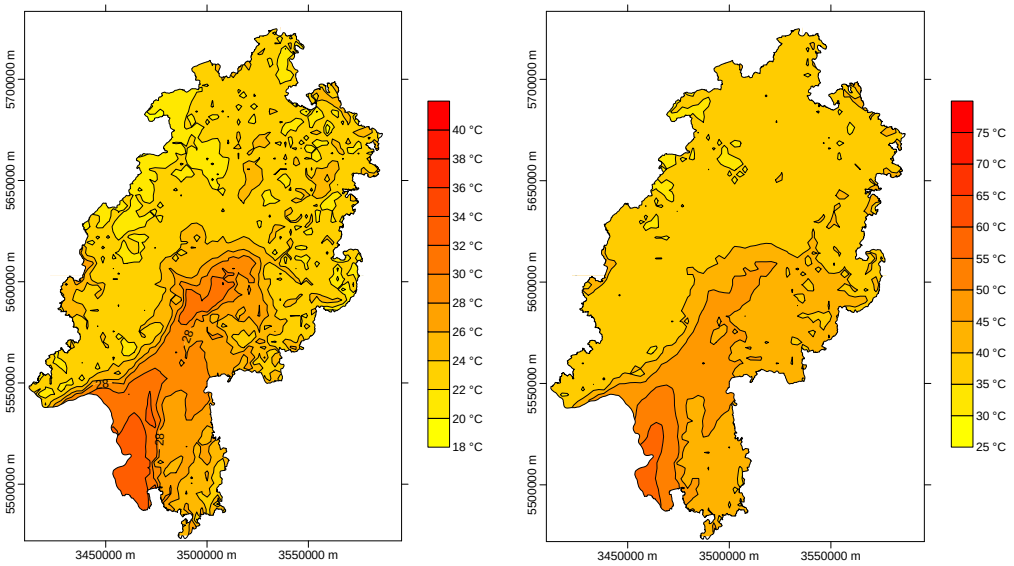

Figure 6: Temperature 500 m (left) and 1000 m (right) below the surface, respectively, based on the FEFLOW numerical heat transport model.

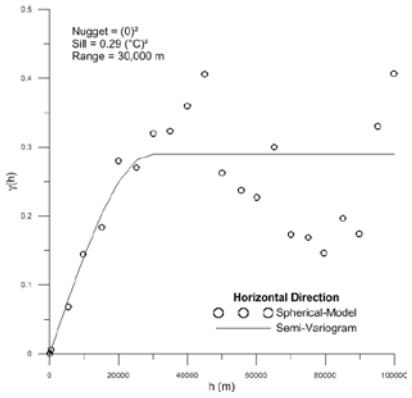

Figure 7: Semi-variogram of the temperature data in horizontal direction (without sub-model Mainzer Becken and Upper Rhine Graben).

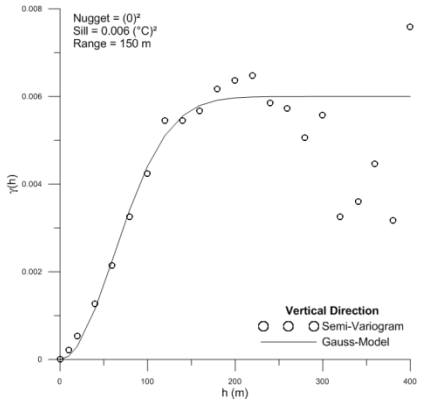

Figure 8: Semi-variogram of the temperature data in vertical direction (only undisturbed continuous logs; all sub-models; measurements deeper 250 m and with more than 15 °C).

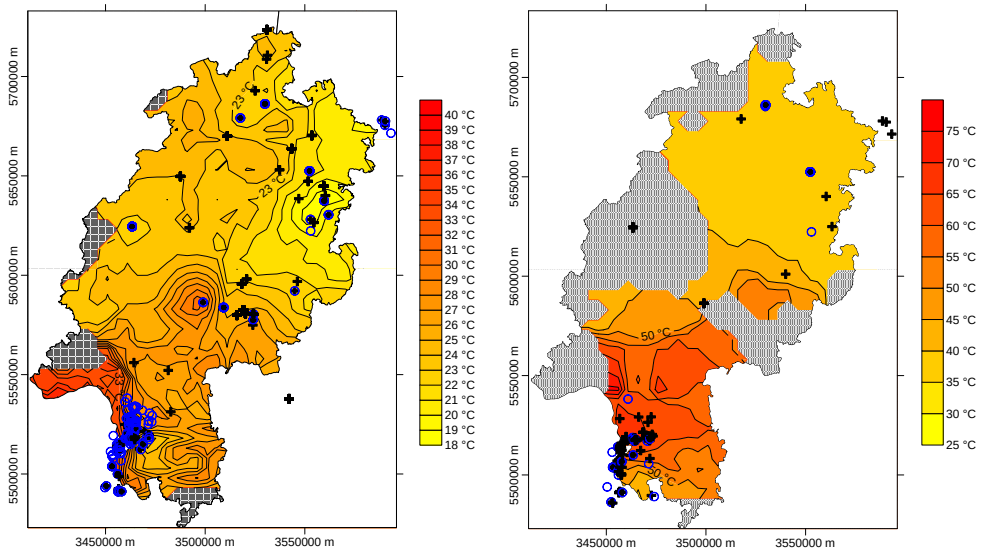

Figure 9: Temperature 500 m (left) and 1000 m (right) below the surface, respectively, based on the 3D quality weighted Kriging.

Table 4: Classification scheme of the subsurface temperature data.

Code	Measurement Description (based on work of the database maintainer, LIAG Hannover)	Estimated Error (K)	n
1	undisturbed logs	0.01	1360
2	disturbed temperature logs	2.4	200
11	BHT with at least 3 temperature measurements taken at different times in the same depth; corrected with a cylinder source approach	0.5	58
21	Production test (DST)	0.5	
12	BHT with at least 2 temperature measurements taken at different times in the same depth; corrected using the Horner plot method	0.7	85
13	BHT with at least 2 temperature measurements taken at different times in the same depth; corrected with an explosion line-source approach	0.7	
14	BHT with one temperature measurement, known radius and time since circulation (TSC)	1.6	46
15	BHT with one temperature measurement, known TSC	1.6	
16	BHT with one temperature measurement, known radius	3	280
17	BHT with one temperature measurement, unknown radius and unknown TSC	3	

4 THM COUPLED MODELING OF A MIDDLE DEEP ENHANCED GEOTHERMAL SYSTEM

As an example for THM coupled modelling of an enhanced geothermal system (EGS) a type model is designed based on the Hessen 3D data.

The dedicated location is at the site of the Institute of Applied Geosciences in Darmstadt in a depth of 2 km.

This site is located directly at the main eastern boundary fault of the Upper Rhine Graben. Several studies of the tectonic settings have been published in the past (recently, Schwarz & Henk, 2005, Peters et al., 2005, Buchmann & Connolly, 2007).

Based on the previously mentioned 3D model of Hessen a submodel was generated. The horizontal extension is 150 m x 150 m. The depth is from 1,990 m till 2,010 m below the surface. The local rocks are granodiorites. The assigned thermo-hydro-mechanical parameters are shown in Table 5.

The horizontal NW-SE orientated stress field is compressive with a pressure of 10 MPa. This is realized in the model with a NW border which is set fixed (Dirichlet X,Y,Z = 0) and a SE border where a Neumann pressure of 10 MPa is assigned. No explicit mechanical boundary conditions are set on the other boundaries. The thermal boundary conditions are fixed temperatures at the top and bottom slices (83.6 °C and 84.4 °C respectively) and a head boundary condition at the outer boundaries of 0 m.

Table 5: The THM parameter used for the application example.

Parameter	Value	Unit
ρc	$2.6 \cdot 10^{6}$	J m^{-3} K^{-1}
λ_{matrix}	2.9	W m^{-1} K^{-1}
n	0.1	-
K	$1 \cdot 10^{-10}$	m s^{-1}
S_s	0.0001	m^{-1}
β	$1 \cdot 10^{-6}$	K^{-1}
Λ=M	20,000	MPa
υ	0.25	-
α_b	1	-

The enhanced geothermal activity is modelled highly simplified with just an injection well in 2,000 m depth where water with a temperature of 54 °C is injected with a flow rate of 259.2 m^3 d^{-1} into the rock which has a temperature of 84 °C. The geothermal gradient is 4 °C/100 m. As a result from the pressure gradient due to the injection as also the change of temperature (ΔT = 30 °C) the stress field is modified. In Figure 10 a general view of the model is shown. In Figure 11 the fluid pressure without (left) and with (right) THM coupling is shown. In case of the THM coupled result the maximum fluid pressure is approximately 10 times higher. In case of FEM results the value at the injection node itself is typically misleading; instead values close to the well should be evaluated.

5 SUMMARY AND OUTLOOK

An open source plug-in for mechanical coupling is available which allows using the popular commercial groundwater and heat- and mass-transport code FEFLOW as a THMC simulator.

First tests of the plug-in demonstrate its potential for geothermal applications. The mechanical induced stress, for instance due to fracturing or during operation, can be modelled and studied.

Depending on the size and amplitudes of the problem the discrete coupling is due to a severe non-linearity a challenging task.

Mechanical computations are costly in terms of memory and CPU time consumption. Future developments will focus on mechanical subgrids to avoid calculations in regions with little interest.

Besides of this several additional improvements for the plug-in code are scheduled for the near future.

The stress-field in the relevant depth of an EGS project is often only roughly known. However, the mechanical properties of the rocks are typically almost unknown. Different ways to improve this situation exist; for instance to deduce on rock-properties based on high-resolution seismic data. Future development will also focus on the application of parameter estimation procedures to improve the validity of the assigned mechanical properties.

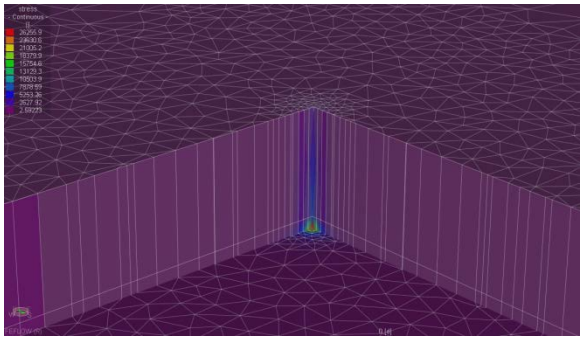

Figure 10: A view of the FEFLOW model after 7 days of cold water injection. Displayed is the respective stress in MPa.

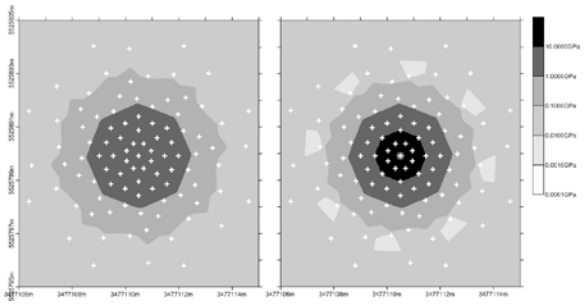

Figure 11: Comparison of the fluid pressure after 7 days of injection of cold water; in the left graph without, and in the right one with mechanical coupling, respectively.

Acknowledgements

The first author was partly funded for this project by the German Science Foundation - DFG (RU 1837/1-1). We have to thank Kristian Bär, Sebastian Homuth and Bishnu Koju who helped while setting up the different models.

REFERENCES

Abriola, L M & Pinder, G F (1982): Calculation of Velocity in Three Space Dimensions from Hydraulic Head Measurements, Ground Water, 20(2): 205-213, doi:10.1111/j.1745-6584.1982.tb02752.x.

Ahola, M P, Thoraval, A & Chowdhury, A H (1996): Distinct Models for the Coupled T-H-M Processes: Theorie and Implementation. In: Coupled Thermo-Hydro-Mechanical Processes of Fractured Media. Mathematical and Experimental Studies. Recent Developments of DECOVALEX Project for Radioactive Waste Repositories. Stephansson, O, Jing, L, Tsang, C-F (Eds.). Developments in Geotechnical Engineering, 79, pp. 181-212. DOI: 10.1016/S0165-1250(96)80026-5

Alberty, J, Carstensen, C, Funken, S A & Klose, R (2002): Matlab Implementation of the Finite Element Method in Elasticity, Computing, 69(3), doi 10.1007/s00607-002-1459-8.

Anderson, M P (2005): Heat as a ground water tracer. Ground Water, 43(6), doi:10.1111/j.1745-6584.2005.00052.x

Arndt, D, Bär, K, Fritsche, J-G, Kracht, M, Sass, I, & Hoppe, A (2011): 3D structural model of the Federal State of Hesse (Germany) for geo-potential evaluation. Z. Dt. Ges. Geowiss., 162(4), 353-369.

Bär, K, Arndt, D, Fritsche, J-G, Götz, A E, Kracht, M, Hoppe, A & Sass, I (2011): 3D-Modellierung der tiefengeothermischen Potenziale von Hessen – Eingangsdaten und Potenzialausweisung. Z. Dt. Ges. Geowiss., 162(4), 371-388.

Bear, J. (1972): Dynamics of Fluids in Porous Media. Dover, New York, NY.

Biot, M A (1941): General Theory of Three-Dimensional Consolidation, Journal of Applied Physics, 12, 155-164.

Buchmann, T J & Connolly, P T, (2007): Contemporary kinematics of the Upper Rhine Graben: A 3D finite element approach. Global Planetary Change 58:287-309.

Bundschuh, J & Suárez Arriaga, M C (2010): Introduction to the Numerical Modeling of Groundwater and Geothermal Systems: Fundamentals of Mass, Energy and Solute Transport in Poroelastic Rocks (Multiphysics Modeling), Taylor & Francis, 522 pages.

Dézes, P, Ziegler, P A (2001): European Map of the Mohorovičić discontinuity, - In: Mt. St. Odile (Eds.): 2nd EUCOR-URGENT Workshop (Upper Rhine Graben Evolution and Neotectonics), France.

DHI-WASY (2012): FEFLOW finite element subsurface flow and transport simulation system—user's manual/reference manual/white papers. Recent release 6.1. Technical Report, DHI-WASY GmbH, Berlin. (http://www.feflow.info).

Diersch, H-J G & Perrochet, P (1999): On the primary variable switching technique for simulating unsaturated saturated flows. Advances in Water Resources, 23(3), doi: 10.1016/S0309-1708(98)00057-8.

Diersch, H-J G, Kolditz O (2002): Variable-density flow and transport in porous media: approaches and challenges. Advances in Water Resources, 25.

Dompierre J, Labbé P, Vallet M-G, Camarero R. (1999): How to Subdivide Pyramids, Prisms and Hexahedra into Tetrahedra, Rapport CERCA R99–78.

Hsieh, P A (1997): Poroelasticity Simulation of Ground-Water Flow and Subsurface Deformation, in Prince, K.R., and Leake, S.A., eds., U.S. Geological Survey Subsidence Interest Group conference—proceedings of the technical meeting, Las Vegas, Nevada, February 14-16,

1995: U. S. Geological Survey Open-File Report 97-47.

Ingebritsen, S E, Sanford, W E & Neuzil, C E (2006): Groundwater in Geologic Processes, 2nd Edition, DOI: 10.2277/ 0521603218, 564 pages.

Kolditz, O, Görke, U-J, Shao, H, & Wang, W (2012). Thermo-Hydro-Mechanical-Chemical Processes in Porous Media: Benchmarks and Examples. Heidelberg: Springer.

Leake, S A, & Hsieh, P A (1997): Simulation of deformation of sediments from decline of ground-water levels in an aquifer underlain by a bedrock step, in Prince, K R, and Leake, S A, eds., U.S. Geological Survey Subsidence Interest Group conference - proceedings of the technical meeting, Las Vegas, Nevada, February 14-16, 1995: U. S. Geological Survey Open-File Report 97-47.

Lee, S H & Ghassemi, A (2011): Three-Dimensional Thermo-Poro-Mechanical Modeling of Reservoir Stimulation and Induced Microseismicity in Geothermal Reservoir; proceedings, 36 Workshop on Geothermal Reservoir Engineering; Stanford University, SGP-TR-191.

Pape, H, Clauser, C & Iffland, 1 (1999): Permeability prediction based on fractal pore space geometry. - Geophysics, Vol. 64/5: 1447-1460;

Peters, G, Buchmann, T J, Connolly, P, van Balen, R T, Wenzel, F, Cloetingh, S A P L. (2005): Interplay between tectonic, fluvial and erosional processes along the Western Border Fault of the northern Upper Rhine Graben, Germany, Tectonophysics, 406(1–2), pp 39-66, doi: 10.1016/j.tecto.2005.05.028.

Rühaak, W, (2006): A Java application for quality weighted 3-d interpolation. Computers & Geosciences 32,1.

Rühaak, W (2013): 3-d interpolation of subsurface temperature data with known measurement error using Kriging. Geothermics (in revision).

Rühaak, W, Rath, V, Wolf, A & Clauser, C, 2008. 3D finite volume groundwater and heat transport modeling with non-orthogonal grids using a coordinate transformation method. Advances in Water Resources 31,3: pp. 513-524.

Rühaak, W, Rath, V & Clauser, C, (2010): Detecting thermal anomalies within the Molasse Basin, Southern Germany. Hydrogeology Journal 18, 8.

Rühaak, W, Bense, V F, Pei, L, Sass, I, 2012a. A FEFLOW IFM plug-in for mechanical coupling, Proceedings, 3rd International FEFLOW User Conference, Berlin, Germany, September, 3.-5.

Rühaak, W, Bär, K, & Sass, I, 2012b. Estimating the subsurface temperature of Hessen/Germany based on a GOCAD 3D structural model - a comparison of numerical and geostatistical approaches. Geophysical Research Abstracts, Vol. 14, EGU2012-5367, 2012, EGU General Assembly, April 23, Vienna.

Rutqvist, J. (2011): Status of the TOUGH-FLAC simulator and recent applications related to coupled fluid flow and crustal deformations, Computers & Geosciences, 37(6): 739-750, doi:10.1016/j.cageo.2010.08.006.

Sass, I, Hoppe, A, Arndt, D & Bär, K (2011): Forschungs- und Entwicklungsprojekt 3D Modell der geothermischen Tiefenpotenziale von Hessen. Report, 218 p., Technische Universität Darmstadt.

Schwarz, M & Henk, A (2005): Evolution and structure of the Upper Rhine Graben – insights from three-dimensional thermomechanical modeling. – International Journal of Earth Sciences, 94/4: 732 – 750.

Si H & Gärtner K (2005): Meshing Piecewise Linear Complexes by Constrained Delaunay Tetrahedralizations, Proceeding of the Fourth International Meshing Roundtable, September 2005.

Smith, I M. & Griffiths, D V (1988): Programming the finite element method, 2nd ed.: Chinchester, John Wiley and Sons, pages 469.

Terzaghi, K (1943): Theoretical Soil Mechanics. John Wiley, New York, 510 pages.

Verruijt, A (1969): Elastic storage of aquifers, in DeWiest, R J M, (ed.), Flow Through Porous Media: New York, Academic Press, p. 331–376.

Wang, H F (2000): Theory of Linear Poroelasticity – with Applications to Geomechanics and Hydrogeology. Princenton University Press, 287 pages.

Wang, W, Kosakowski, G & Kolditz, O (2009): A parallel finite element scheme for thermo-hydro-mechanical (THM) coupled problems in porous media, Computers and Geosciences, 35(8), pp 1631-1641. doi 10.1007/s00466-009-0445-9.

Watanabe, N, Wang, W, McDermott, C, Taniguchi, T & Kolditz, O (2010): Uncertainty analysis of thermo-hydro-mechanical coupled processes in heterogeneous porous media, Computational Mechanics,45(4), pp. 263-280, doi: 10.1007/s00466-009-0445-9.